Similarity-Based Extraction of Individual Networks from Gray Matter MRI Scans

Betty M. Tijms[1,2], Peggy Seriès[2], David J. Willshaw[2] and Stephen M. Lawrie[1]

[1]Division of Psychiatry, University of Edinburgh, Edinburgh EH10 5HF, UK and [2]Institute for Adaptive and Neural Computation, School of Informatics, University of Edinburgh, Edinburgh EH8 9AB, UK

Address correspondence to Betty M. Tijms, The University of Edinburgh, Royal Edinburgh Hospital, 7th Floor Kennedy Tower, Edinburgh EH10 5HF, UK. Email: b.m.tijms@sms.ed.ac.uk.

The characterization of gray matter morphology of individual brains is an important issue in neuroscience. Graph theory has been used to describe cortical morphology, with networks based on co-variation of gray matter volume or thickness between cortical areas across people. Here, we extend this research by proposing a new method that describes the gray matter morphology of an individual cortex as a network. In these large-scale morphological networks, nodes represent small cortical regions, and edges connect regions that have a statistically similar structure. The method was applied to a healthy sample ($n = 14$, scanned at 2 different time points). For all networks, we described the spatial degree distribution, average minimum path length, average clustering coefficient, small world property, and betweenness centrality (BC). Finally, we studied the reproducibility of all these properties. The networks showed more clustering than random networks and a similar minimum path length, indicating that they were "small world." The spatial degree and BC distributions corresponded closely to those from group-derived networks. All network property values were reproducible over the 2 time points examined. Our results demonstrate that intracortical similarities can be used to provide a robust statistical description of individual gray matter morphology.

Keywords: graph theory, gray matter, individual networks, magnetic resonance imaging, morphometry

Introduction

This paper presents a new method that is used to construct networks from individual cortices based on intracortical similarities in gray matter morphology. In these networks, the nodes represent small regions of gray matter with their 3D structure intact, and edges are placed between regions that show statistical similarity. Representing the morphology of the brain as a network has the advantage that the surface structure can be described statistically with tools from graph theory. Recent studies have shown that it is possible to construct morphological networks using correlations between cortical areas in cortical thickness or volume across people (He, Chen, et al. 2007; Bassett et al. 2008; Chen et al. 2008; He et al. 2008) and that such networks can be used to distinguish between (clinical) groups (e.g., Wright et al. 1999; McAlonan et al. 2005; Mechelli et al. 2005; Mitelman et al. 2005; Thompson et al. 2005; Lerch et al. 2006; He, Wang, et al. 2007; Bassett et al. 2008; Colibazzi et al. 2008; He et al. 2008; Liu et al. 2008; Bernhardt et al. 2009; Modinos et al. 2009).

Although graph theory has provided a statistical framework to study cortical morphology, it remains unclear as to what are the most appropriate measures to define nodes and edges in morphological networks (Bullmore and Sporns 2009). Most studies choose as the network nodes anatomical areas that are connected when they covary in thickness or volume across individuals (He, Chen, et al. 2007; Bassett et al. 2008; Chen et al. 2008; He et al. 2008). Such an approach requires mapping of individual brains into a standard space and requires prior models to extract anatomical regions. These requirements might obscure subtle structural differences that are of particular interest in clinical populations. Therefore, it is important to study gray matter networks derived from individual cortices. In order to do this, we propose to represent the cortical morphology of individual subjects as networks, using information about the similarity of gray matter structure within the cortex.

Covariation of cortical morphology might be related to anatomical connectivity, induced by mutually trophic influences (Pezawas et al. 2004) or caused by experience driven plasticity (e.g., Andrews et al. 1997; Draganski et al. 2004; Mechelli et al. 2004). Lerch et al. (2006) were the first to show that cortical thickness correlations qualitatively match a diffusion tensor imaging (DTI) traced track, implying that anatomical connectivity could be measured indirectly using information from the cortical surface. In animal tracer studies, it has been found that cortical thickness, folding, and neuronal density can predict anatomical connectivity (Barbas 1986; Barbas and Rempel-Clower 1997; Dombrowski et al. 2001). These studies suggest that similarity in thickness and folding might be an indication of connectivity between cortical areas.

To our knowledge, only a few studies have tried to quantify morphological covariation in individual brains (Andrews et al. 1997; Kennedy et al. 1998). For example, Andrews et al. (1997) found that within individual brains, the gray matter of the lateral geniculate nucleus, the optical tract, and the primary visual cortex covary in volume.

Here, we further extend these studies by demonstrating our method in a sample of 14 healthy subjects who had been scanned at 2 different time points, as reported previously (Moorhead et al. 2009; Gountouna et al. 2010). We studied the graph theoretic properties of the networks obtained and compared the results with previous studies that constructed networks from group morphological, functional, and white matter magnetic resonance imaging (MRI) data. Finally, the robustness of the method was assessed by measuring the stability of the network statistics between 2 scanning sessions.

Materials and Methods

The following sections describe 1) the new method in detail, 2) the sample to which the method was applied, 3) the data acquisition details, 4) the preprocessing procedures applied to the scans, 5) the statistics applied to the networks, and 6) the reproducibility procedure.

Extraction of Networks from Individual Gray Matter Segmentations

Figure 1 shows a schematic overview of the method that is completely automated and data driven and thus requires no a priori hypotheses about the regions of interest. First, the method divided the gray matter segmentation of an individual brain starting from the first nonempty voxel into $3 \times 3 \times 3$ voxel cubes, in a manner similar to methods that match scans from different modalities (Borgefors et al. 1997; Ourselin et al. 2000). Using cubes kept the 3D structure of the cortex intact, thereby using spatial information from the MRI scan in addition to the gray matter values in the voxels. By keeping the spatial information intact, the cubes contain a quantity that reflects the local thickness and folding structure of the cortex. In contrast, cortical volume measures only the number of voxels at a location and thus does not include information concerning the spatial relationship between voxels. Similarly, cortical thickness measures do not contain information about the 3D folding structure of the cortex.

The size of the cubes was constrained by 2 factors: 1) The minimum spatial resolution that still captures cortical folding has been shown to be 3 mm (Kiselev et al. 2003) and 2) Practical computational limitations exist with large matrices. Therefore, we used a cube size of $3 \times 3 \times 3$ voxels, corresponding to $6 \times 6 \times 6 \ \text{mm}^3$.

Each cube is represented by a different node v in the network. A network contained on average 6977 nodes (standard deviation [SD] = 783.92, over both subjects and runs). To construct a network, 2 nodes v_j and v_m were connected when their similarity metric exceeded a certain threshold. We chose the correlation coefficient to quantify the structural similarity between 2 cubes because it is simple to understand

and implement while at the same time fast to compute (Lewis 1995; Nikou et al. 1999; Weese et al. 1999; van Court et al. 2005; Penney et al. 2008). Additionally, the correlation coefficient does not require centering of the data because it is normalized by the SD of the cubes. The numerator of the correlation coefficient r_{jm} between cubes v_j and v_m calculates the sum over the product of the differences between the cubes' values at each voxel location $i = 1, 2, \ldots n$ for n voxels (after subtraction of the cubes' average values, respectively, $\bar{v}_j$ and $\bar{v}_m$). The denominator of the correlation coefficient is the product of the cubes' SDs:

$$r_{jm} = \frac{\sum_{i=1}^{n}\left(v_{ji} - \bar{v}_j\right)\left(v_{mi} - \bar{v}_m\right)}{\sqrt{\sum_{i=1}^{n}\left(v_{ji} - \bar{v}_j\right)^2}\sqrt{\sum_{i=1}^{n}\left(v_{mi} - \bar{v}_m\right)^2}}. \tag{1}$$

Cubes with zero variance were excluded (average $< 0.01\%$). Given that the cortex is a curved object, 2 similar cubes could be located at an angle from each other, which could decrease their similarity value. As the cubes were constructed from discrete MRI data, we have rotated each seed cube v_j by an angle θ with multiples of $45°$ and reflections over all axes to find the maximum correlation value with target cube v_m:

$$r_{jm}^{\max} = \underset{\theta}{\arg\max}\left(\frac{\sum_{i=1}^{n}\left(v_{ji}(\theta) - \bar{v}_j\right)\left(v_{mi} - \bar{v}_m\right)}{\sqrt{\sum_{i=1}^{n}\left(v_{ji}(\theta) - \bar{v}_j\right)^2}\sqrt{\sum_{i=1}^{n}\left(v_{mi} - \bar{v}_m\right)^2}}\right). \tag{2}$$
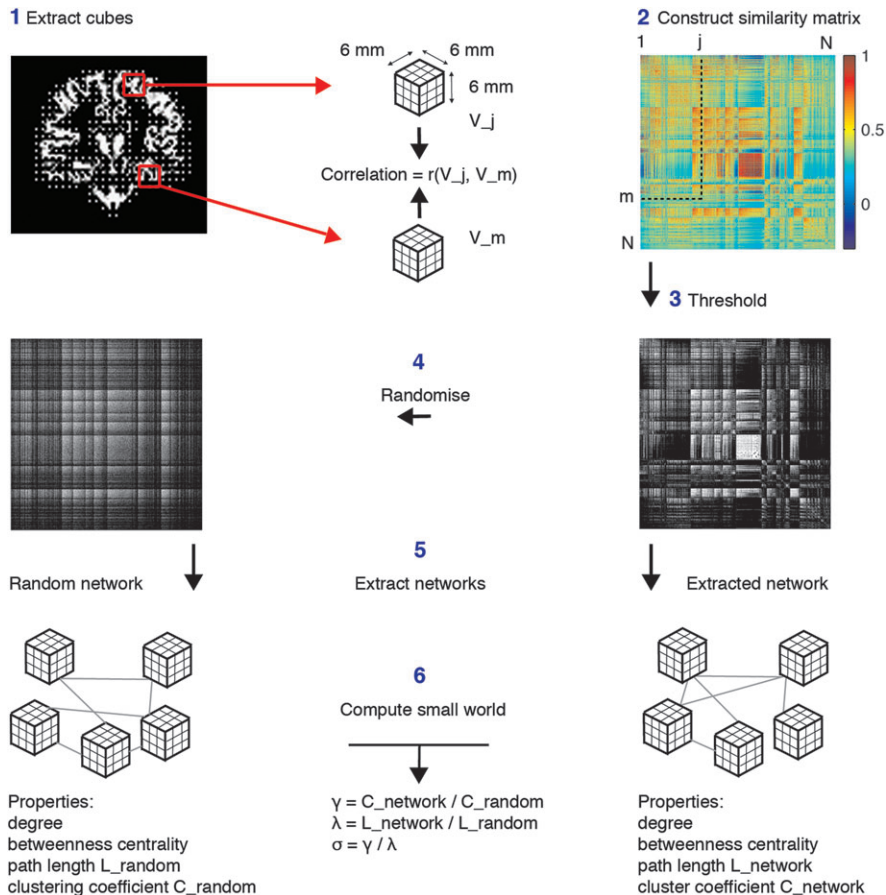
Figure 1. General pipeline of the extraction of individual networks. After preprocessing, the gray matter was divided into $3 \times 3 \times 3$ voxel cubes, visualized by a white voxel in the centre of each cube (1). The red arrows point to 2 example cubes v_j and v_m (note that the cubes were magnified for illustration purposes). The similarity between all N cubes within a scan was computed with the correlation coefficient, storing the result in a matrix with 1 to N rows and columns (2). In (3), the similarity matrix was binarized, with a threshold that ensured a 5% chance of spurious connections for all individuals (corresponding to a significance level of $P = 0.05$ corrected for multiple comparisons by an FDR technique using an empirical null distribution). Twenty random matrices that kept intact the spatial degree distribution were generated for each binarized similarity matrix (4). Finally, we constructed the networks and computed the degree, BC, the path length, clustering coefficient, and small world property of the extracted and random networks (6).

In theory, other angles could be chosen as well. However, then interpolation between voxels would be necessary, which adds noise to the data and entails computational difficulties. In a simulation study, using a simplified model for the structural MRI data, we found that using angles with multiples of 45° recovered 99% of the similarities (see Supplementary Material, Supplementary Figure 1), suggesting that these angles are sufficient to correct for rotation.

Binarization of the Similarity Matrix

The similarity matrices were binarized to construct undirected and unweighted graphs. The graphs were undirected because it is not feasible to infer causality from correlations. Although continuous weights would contain the most information (Barrat et al. 2004), the present study assessed only the basic network topology, and therefore, the networks were binarized.

To binarize the networks, a threshold was determined for each individual based on the significance of the correlations. Because correlations were computed between on average 6977 nodes and maximized for rotation and reflection, it was necessary to correct for multiple comparisons when determining the threshold. The false discovery rate (FDR) technique with the use of an empirical null model was employed to correct for multiple comparisons (Benjamini and Hochberg 1995; Benjamini and Yekutieli 2001; Noble 2009; see Supplementary Material for full description). Briefly, an FDR is the proportion of false positives in a set of significant scores. This proportion corresponds to the area greater than a threshold value in the null model score distribution. An advantage of this approach is that all individuals will have the same 5% chance of spurious correlations.

After the threshold was determined, it was used to binarize the networks where the presence of an edge was indicated by 1 (a correlation greater than the threshold) and absence of an edge indicated by 0 (a correlation lower than the threshold). In this study, we use the word "connections" to refer to these edges, as they connect the nodes in our networks. These connections should not be confused with anatomical connections and indicate whether any 2 cubes have statistically similar gray matter morphology. We define the sparsity of the networks as the connectivity density within a matrix. This was simply quantified as the percentage number of existing edges compared with the maximum number of edges possible ($N(N-1)$, where N is the number of nodes).

Participants

The data used here were previously collected for the CaliBrain study (Moorhead et al. 2009; Gountouna et al. 2010). Fourteen healthy volunteers (9 males, mean age at first scan 34.80, SD = 8.23) participated in CaliBrain. All participants were native English speakers, right handed (self-reported), had no history of substance abuse, nor a history of diagnosed neurological disorder, major psychiatric disorder, or treatment with psychotropic medication. All participants provided written informed consent, and the study was approved by the appropriate research ethics committee.

Data Acquisition

The scans were acquired at the University of Edinburgh (The Division of Psychiatry and the Scottish Funding Council Brain Imaging Research Centre within the Centre for Clinical Brain Sciences). The scanner was manufactured by General Electric (GE Healthcare, Milwaukee, WI) and had a field strength of 1.5 T. The subjects were scanned twice within a 6-month period. At each visit, a high resolution T_1-weighted scan was acquired using a 3D inversion recovery-prepared fast gradient echo volume sequence with a coronal orientation and the following parameters: repetition time of 8.2 ms, echo time of 3.3 ms, inversion time of 600 ms, flip angle of 15°, matrix size of 256 × 256, field of view of 220 mm², and 128 slices with 1.7 mm thickness without a gap, resulting in voxels with size 0.86 × 1.7 × 0.86 mm³.

Preprocessing and Segmentation

Twenty-eight T_1-weighted scans were preprocessed using SPM5 (Wellcome Department of Cognitive Neurology and collaborators,

Institute of Neurology, London, UK: http://www.fil.ion.ucl.ac.uk/spm/software/spm5) with Matlab version 7.3.0.298 R2006b (Mathworks, Natick, MA) on a Dell Precision 690 workstation with RedHat Enterprise Linux WS v.4. First, the origin of all scans was manually set to the anterior commissure. Then, the scans were segmented with the VBM5 toolbox (University of Jena, Department of Cognitive Neurology, C. Gaser: http://dbm.neuro.uni-jena.de/vbm) using a Hidden Markov Random Field (HMRF), without SPM priors and the option "lightly cleaned" (as defined by VBM5) into gray matter, white matter, and cerebral spinal fluid in native space. The HMRF used spatial constraints based on neighboring voxels in a 3 × 3 × 3 voxel cube, increasing the accuracy of segmentation. After segmentation, the data were resliced to 2 × 2 × 2 mm³ voxels. All further data analyses were implemented in Matlab version 7.3.0.298 R2006b (unless specified otherwise).

Network Metrics

This section describes in detail the following metrics that were computed from the networks: the degree, the minimum path length, the clustering coefficient, the small world property, and the betweenness centrality (BC).

Degree k
The number of connections each node v has.

Minimum and Average Path Length
The minimum path length $L_{i,j}$ between 2 nodes v_i and v_j is the minimum number of edges that needs to be traveled to go from a node v_i to node v_j. The minimum shortest path length of a node v_i is the average of its shortest path lengths to all other nodes (Dijkstra 1959; Watts and Strogatz 1998):

$$L_i = \frac{\sum_{j=1, j \neq i}^{N} L_{i,j}}{N}. \qquad (3)$$

The minimum path length L of a network is the average of L_i over all N nodes (Dijkstra 1959; Watts and Strogatz 1998):

$$L = \frac{\sum_{i=1}^{N} L_i}{N}. \qquad (4)$$

Clustering C
The clustering coefficient c_i of a node v_i is defined as the number of edges k_j between its direct neighbors (denoted by subgraph g_i) divided by the total number of all possible edges k_{g_i} in g_i (Luce and Perry 1949; Watts and Strogatz 1998):

$$c_i = \frac{\sum_{j,k \in g_i} k_j}{k_{g_i}(k_{g_i} - 1)/2}. \qquad (5)$$

The clustering coefficient C_{network} of the network is the average clustering coefficient c_i over all N nodes:

$$C_{\text{network}} = \frac{\sum_{i=1}^{N} c_i}{N}. \qquad (6)$$

Small World (σ)
A network is defined to have the small world property when it shows more clustering than a random network, its average minimum path length remaining similar to that of a random graph (Watts and Strogatz 1998; Humphries et al. 2006). For each network b, random networks were generated by rearranging the edges while keeping the degree distribution intact (Maslov and Sneppen 2002) to compute an average $\bar{C}_{\text{random}}$ and $\bar{L}_{\text{random}}$ ($\bar{C}_{\text{random}} = 1/b \sum_{i=1}^{b} C_{\text{random}_i}$ and $\bar{L}_{\text{random}} = 1/b \sum_{i=1}^{b} L_{\text{random}_i}$). Given the large size of the networks, a value of $b = 20$ enabled computation in a reasonable time (in total 28 × 20 = 560 random networks). The division of C_{network} by $\bar{C}_{\text{random}}$ is denoted by γ (Watts and Strogatz 1998; Humphries et al. 2006):

$$\gamma = \frac{C_{\text{network}}}{\bar{C}_{\text{random}}}. \qquad (7)$$

For a network to contain the small world property, it is required that γ is larger than 1. The division of L_{network} by $\bar{L}_{\text{random}}$ is denoted by λ (Watts and Strogatz 1998; Humphries et al. 2006):

$$\lambda = \frac{L_{\text{network}}}{\bar{L}_{\text{random}}}. \qquad (8)$$

For a network to contain the small world property, it is required that λ is approximately equal to 1. The small world property (σ) is defined as the division of γ and λ (Humphries et al. 2006):

$$\sigma = \frac{\gamma}{\lambda}. \qquad (9)$$

When the small world property (σ) of a network is higher than 1, it indicates that the topology lies between that of a completely regular (i.e., a lattice) and a completely random network. If one connects all the nodes with an arbitrary number of their neighbors, the result will be a fully connected network that is one big cluster. In contrast, connecting nodes randomly result in a network with minimal clustering and a much lower average minimum path length. Networks with the small world property can be placed between these 2 extremes and are fully connected with minimal wiring length due to a few long-range connections between clusters (e.g., Watts and Strogatz 1998; Humphries et al. 2006). Such architecture is efficient because clusters can be highly specialized units of nodes that are densely connected, and information can be exchanged between clusters via their long-range connections (Milgram 1967; Watts and Strogatz 1998; Albert and Barabási 2002; Newman 2003; Sporns et al. 2004, 2005). Several studies have shown that networks extracted from imaging data contain the small world property (e.g., Achard et al. 2006; Bassett and Bullmore 2006; He et al. 2008; van den Heuvel et al. 2008; Gong et al. 2009). The anatomical architecture of the macaque and cat cortex based on tracer studies is also small world (Sporns and Zwi 2004).

Betweenness Centrality

BC Quantifies the fraction of shortest paths $s_{j,m}$ between nodes v_j and v_m that run through a node v_i in the total network G (Freeman 1977):

$$\text{BC}(i) = \sum_{j \neq m \neq i \in G} \frac{s_{j,m}(i)}{s_{j,m}}. \qquad (10)$$

The BC of a graph is the average over all nodes.

Finally, hubs were defined as nodes with a degree and/or BC value higher than one SD above the corresponding average value in the network.

Reproducibility

The intraclass correlation coefficient (ICC) was used to estimate the reproducibility of all graph theoretic measures. McGraw and Wong (1996) defined the ICC as the ratio of the variance between subjects ($\sigma^2_{\text{between}}$) to the total variance in test scores ($\sigma^2_{\text{between}} + \sigma^2_{\text{within}}$):

$$\text{ICC} = \sigma^2_{\text{between}} / \left(\sigma^2_{\text{between}} + \sigma^2_{\text{within}} \right). \qquad (11)$$

The within-subject variance (σ^2_{within}) gives an indication of measurement error between repeated measurements. The ICC is close to 1 if the measurements of 2 repeated scans are consistent for each subject in the sample. Computation of the ICC was performed in R version 2.10 (http://cran.r-project.org, using the "irr" package).

Results

Threshold

The threshold used in the binarization process corresponded to a P value of 0.05 corrected for multiple comparisons with an FDR (Benjamini and Hochberg 1995; Benjamini and Yekutieli 2001; Noble 2009). Using this threshold ensured that there was the same chance of including maximally 5% spurious con-

nections in any network. None of the networks had isolated nodes, in other words, all the networks were fully connected. The binarized anatomical connection matrices had an average sparsity of 23% (SD = 1%, over runs and over subjects).

Graph Properties of the Individual Networks

For the first time, this method permitted the investigation of morphological networks extracted from individual brains. Initially, to assess whether the extracted networks were small world, their average clustering coefficient and average minimum path length were compared with those from the random networks. Figure 2a shows that the individual clustering coefficients of the extracted networks were higher than those from the randomized networks (one-sided paired t-tests, range of t values: min = 55.78; max = 147.92; all $P < 2.2 \times 10^{-16}$). Figure 2b shows that the individual average minimum path lengths were significantly higher than those from the random networks (two-sided paired t-test, t values range: min = 56.11; max = 88.57; all $P < 2.2 \times 10^{-16}$). In addition, because the ratio of the average path lengths of the extracted and random networks was close to 1 (range λ: min = 1.04; max = 1.06), all networks had the small world property. To demonstrate that the individual measures can be combined into a single group measure, the clustering coefficient and minimum path length averaged over all individuals are shown in Figure 2c,d. Similar to
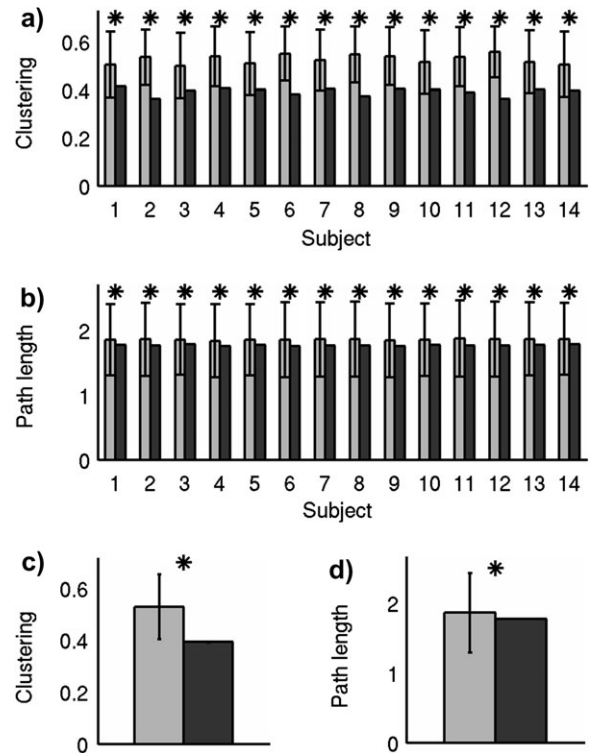
Figure 2. A network contains the small world property when its clustering coefficient is higher than random networks while its path length is similar. We plotted the average clustering coefficient (a) and minimum path length (b) for the individually extracted networks (gray) and their randomized versions (black). The stars indicate a significant difference of $P < 0.05$ tested with a paired t-test between a network and the average nodal values of its corresponding random network. Next, we plotted the average clustering coefficient and minimum path length averaged over all networks (c) and their randomized versions (d). All networks had the small world property. The stars indicate a significant difference with $P < 0.05$ tested with paired t-tests between the average network values and their random networks.

the individual cases, the clustering coefficient averaged over subjects was higher than the random clustering coefficients (one-sided paired t test: $t_{13} = 15.73$, $P = 3.83 \times 10^{-10}$). The minimum path length averaged over subjects was also higher than the random path length (two-sided paired t-test: $t_{13} = 30.73$, $P = 1.60 \times 10^{-13}$). However, the ratio was close to 1 (mean $\lambda = 1.05$, SD = 0.01), thus demonstrating that the networks were small world.

Because the current analysis was performed in native space, all networks differed in size. Previous studies have shown that network properties are dependent on the number of nodes, the degree, and the sparsity of a network (e.g., He, Chen, et al. 2007; Bassett et al. 2008, 2010; He et al. 2008; Fornito et al. 2010; van Wijk et al. 2010; Zalesky et al. 2010). To investigate such relationships, we computed pairwise correlations between all network measures (see Supplementary Table 1). Briefly, larger networks had a larger average degree ($r = 0.96$, $P = 4.12 \times 10^{-8}$), a smaller minimum path length ($r = -0.59$, $P = 0.03$), and a higher betweenness coefficient ($r \approx 1$, $P = 2.37 \times 10^{-14}$). Furthermore, sparsity had a strong positive relationship with the clustering coefficient ($r = 0.91$, $P = 5.75 \times 10^{-6}$) and the small world property ($r = 0.61$, $P = 0.02$), similar to results previously reported in other studies (e.g., He et al. 2008). There was, however, no relation between sparsity and the number of nodes or degree.

To investigate whether the present method produced networks with properties comparable to previous studies, we summarized in Table 1 all the morphological studies that reported network properties in healthy individuals that we are aware of (He, Chen, et al. 2007, 2008; Bassett et al. 2008; Sanabria-Diaz et al. 2010; Yao et al. 2010; Zhu et al. 2010) for a sparsity similar to that found in our study (23%). As all morphological studies have a smaller network size than the present study, only the clustering and small world coefficients

can be compared directly with our study since these measures were significantly related to the sparsity and not to the size of the networks. In addition, we included studies that extracted networks of a comparable size to the present study from functional (Eguíluz et al. 2005; van den Heuvel et al. 2008; Zhang et al. 2009, 2010; Fornito et al. 2010; Hayasaka and Laurienti 2010) and white matter MRI (Hagmann et al. 2007; Zalesky et al. 2010). Their network properties were summarized for a sparsity of approximately 23% when this level was available and otherwise for the maximum sparsity.

Only two studies in Table 1 reported networks that were comparable to the present study in both size and sparsity (van den Heuvel et al. 2008; Fornito et al. 2010). These 2 functional MRI studies were highly similar to the present study over all network properties. This suggests that correlations in resting-state functional MRI are organized similarly to our intracortical morphological correlations.

When comparing the present study with other morphometric studies, its clustering coefficient (0.53) was slightly higher than previously reported values (min = 0.25; max = 0.49). The value of the small world property of the present networks (1.28) fell within a small range of previously reported values (min = 1.17; max = 1.47), suggesting that intracortical similarities might be organized similarly to correlations in thickness or volume between cortical areas assessed over subjects.

The present small world property was strikingly lower than the remaining functional studies (Eguíluz et al. 2005; Zhang et al. 2009, 2010; Hayasaka and Laurienti 2010) and 2 white matter studies (Hagmann et al. 2007; Zalesky et al. 2010). Finally, Table 1 shows that the property values of morphological networks varied within a narrow range, while those from functional and white matter MRI varied over a wider range (e.g., the small world values ranged between 1.28 and 168.54).

Table 1

Graph measures from our study and for comparison from other morphological, functional, and white matter MRI network studies

| Study	N	C	L	γ	λ	σ	s (%)
Morphological							
Present study ($n = 14$)	6982	0.53	1.86	1.35	1.05	1.28	23
He, Chen, et al. (2007) ($n = 124$), cortical thickness	52	nr	nr	≈1.5	≈1.15	≈1.3	≈23
He et al. (2008) ($n = 97$), cortical thickness	54	≈0.3	≈1.6	≈1.35	≈1	≈1.35	23
Bassett et al. (2008) ($n = 259$), gray matter volume	104	≈0.25	nr	nr	nr	≈1.18	23
Sanabria-Diaz et al. (2010) ($n = 186$), comparison of cortical thickness and cortical surface descriptors.	82 AAL—Area	≈0.3	≈1.81	nr	nr	≈1.28	22
	56 Jacob—Area	≈0.28	≈1.84	nr	nr	≈1.23	22
	82 AAL—Thickness	≈0.29	≈1.81	nr	nr	≈1.23	22
	56 Jacob—Thickness	≈0.27	≈1.84	nr	nr	≈1.18	22
Yao et al. (2010) ($n = 98$), gray matter volume	90	≈0.49	≈1.89	≈1.62	≈1.1	≈1.47	23
Zhu et al. (2010) ($n = 428$), gray matter volume	90 (AAL)	≈0.26	nr	≈1.20	≈1.03	≈1.17	23
MRI studies that analyzed networks with $N > 1000$							
Functional							
Eguíluz et al. (2005) ($n = 7$), Averaged values over 2 tasks; finger-tapping task and listening to music	4891	0.15	6.0	168.54	1	168.54	0.08
van den Heuvel et al. (2008) ($n = 28$), resting-state functional MRI 0.01–0.09 Hz	10 000	≈0.52	≈1.75	≈1.9	≈1.03	≈1.85	20
Zhang et al. (2009) ($n = 1$), finger movement task	1397	0.54	2.59	11.25	1.3	8.65	4.80
Fornito et al. (2010) ($n = 30$), resting-state functional MRI 0.04–0.08 Hz	4320	≈0.62	≈1.9	≈1.35	≈1.06	≈1.28	20
Hayasaka and Laurienti (2010) ($n = 10$), resting-state functional MRI 0.009–0.08 Hz	16 000	0.24	3	≈7	≈1.22	6	0.79
Zhang et al. (2010) ($n = 4$), finger movement task	2255	0.46	5.39	26.74	2.14	12.50	1.44
White matter							
Hagmann et al. (2007) ($n = 1$), DSI	4052	0.3	3	20	1	20	0.61
Zalesky et al. (2010) ($n = 3$), comparison of DTI and HARDI	4000 DTI	≈0.28	≈8.85	111.7	1.8	62.05	≈0.25
	4000 HARDI	≈0.24	≈6.15	77.5	1.4	55.36	≈0.28

Note: N, the number of nodes in the networks; C, the average cluster coefficient; L, the average minimum path length; γ, the ratio of the networks cluster coefficient and that of its randomized version; λ, the ratio of the average minimum path length of the network and that of its randomized version; σ, the small world coefficient (γ/λ); and finally, s, the sparsity of the network in percentage connections. nr is "not reported". AAL is the Automatic Anatomical Labeling atlas (Tzourio-Mazoyer et al. 2002). We tried to get measurements for the network values that corresponded to a similar sparsity as the present study (23%), if this was not possible, we chose the maximum sparsity available. We did not include the studies by van den Heuvel et al. (2009), Yuan et al. (2010), Telesford et al. (2010), and Fransson et al. (2011) that also investigated network sizes of >1000 because they did not report network sparsity or network property values.

In particular, the value of γ in those studies was 1–100 times higher than in our study (min = 1.35; max = 168.54), resulting in higher values for σ. This variation might be explained by differences in procedures used to construct random networks but also by the low sparsity of these networks (min = 0.08%; max = 0.79%) in comparison with the present study (23%). Since the functional and white matter networks are comparable in size, this leaves an interesting question as to whether keeping sparsity constant would give rise to more similar networks across different scanning modalities.

Spatial Distribution of the Degrees within the Networks

We tested how the spatial distribution of the number of connections (i.e., degree) of the nodes in a network compared with the distribution reported in a previous study that derived cortical thickness correlations between anatomical areas in

groups (Lerch et al. 2006). In that study, the associative cortices were found to have the highest correlations in thickness with other regions of the brain. Figure 3a shows for each of the 14 subjects a slice from the medial right hemisphere with the standardized degree for all cubes resulting in a spatial distribution of the degree values. Each square is a side of a cube, with warmer colors indicating a higher degree. The figure shows that all individuals had a unique spatial distribution of the degree values. To demonstrate that it is possible to combine these networks into a single group network, the average of the individual patterns was plotted after warping these to a standard space and averaging standardized degree values over subjects (Fig. 3b). Finally, we also used the SPM tool SurfRend to plot the group result on an inflated surface (Fig. 3c, thresholded for computational reasons to include just the hubs, i.e., nodes with
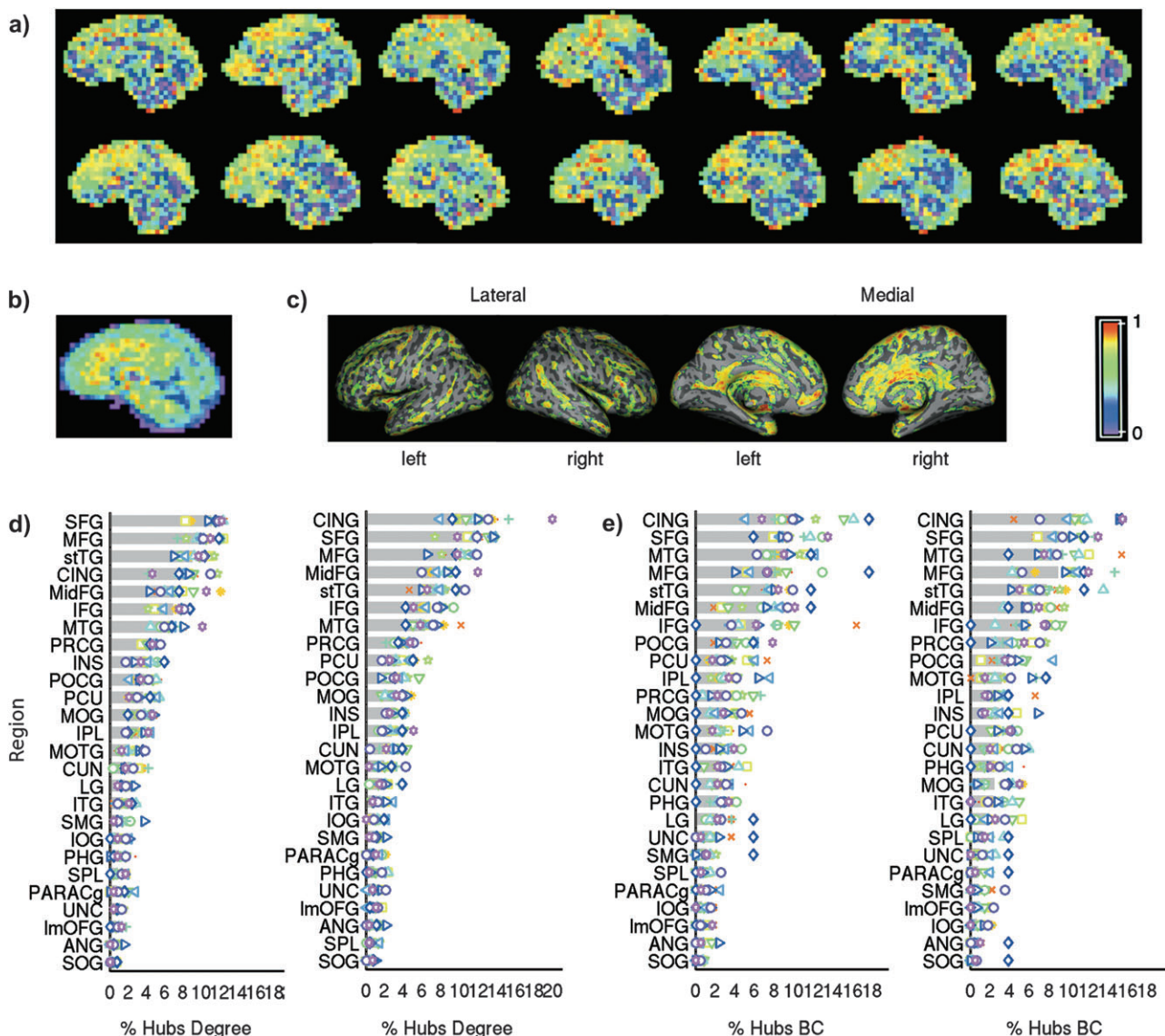
Figure 3. (a) A plot of the degree of all cubes for one slice (right medial hemisphere) from each individual subject. The degrees were standardized by their maximal value. Warmer colors indicate that a cube has more structural similarities with other cubes in the brain than cubes with cooler colors. (b) Shows the group average of the degree patterns after warping to standard Montreal Neurological Institute space, which supports that most subjects have hubs along the right medial surface of the brain. (c) Shows the spatial distribution of hubs (nodes with a degree higher than one SD above the mean) averaged over all 14 subjects and plotted on a surface. To quantify the spatial degree distribution, we plotted the average percentage of hubs for both hemispheres based on the degree (d) and on the BC (e) for 26 anatomical areas (Supplementary Table 2 lists full names). Each symbol and color combination in all bar plots represents an individual percentage of hubs in that area.

a degree higher than one SD above the mean). We further quantified the individual spatial degree patterns by assessing the spatial distribution of hubs over 26 distinct anatomical areas per hemisphere extracted with an anatomical mask (constructed with the WFU Pick-Atlas, http://www.fmri.w-fubmc.edu, Advanced Neuroscience Imaging Research Core. See Supplementary Table 2 for a list of the anatomical areas, their abbreviations, and sizes). The anatomical mask incorporated approximately the same regions as used in previous studies that extracted morphological networks using cortical thickness (He, Chen, et al. 2007; Chen et al. 2008; He et al. 2008). The mask was warped to the individual native spaces, using the inverted parameter matrices from normalization of the scans to standard space. Next, for each subject, the degree hubs (nodes with a degree higher than one SD above the mean, within a subject) were identified, and the percentage of hubs was calculated for each anatomical area. The bar plot in Figure 3d confirms that on average 77% of the hubs were located in the prefrontal (superior, medial, middle, and inferior frontal gyri, precentral gyrus), the cingulate posterior regions (post-central gyrus and precuneus), and the insula and temporal areas (superior, transverse, and middle temporal gyri). For comparison with other studies, we also plotted the spatial distribution of the hubs for BC in Figure 3e (hubs defined as having a BC value that is higher than one SD above the mean BC), which resulted in a similar spatial distribution with 77% of the hubs in the same areas as Figure 3d. In Table 2, these areas are summarized with their corresponding average degree and BC. Table 2 also indicates other studies that found the same areas with structural MRI using cortical volume (Bassett et al. 2008) or cortical thickness (He, Chen, et al. 2007; Chen et al. 2008), white matter (Iturria-Medina et al. 2008; Gong et al. 2009), and functional MRI (Achard et al. 2006; Buckner et al. 2009). Our hub areas have all been reported by at least one of the studies above. However, we found a strong relationship between the percentage of hubs and the region size in both

hemispheres (left hemisphere: $r = 0.95$, $P = 1.72 \times 10^{-13}$; and right hemisphere: $r = 0.95$, $P = 1.65 \times 10^{-13}$), which might explain why these areas were also reported as hubs in other studies (also see: Bassett et al. 2010).

Reproducibility of the Measures

Finally, we assessed the robustness of the method by measuring the network metrics for scans that were acquired at 2 different time points in Figure 4. The number of nodes was highly stable (ICC = 0.98, $P = 3.48 \times 10^{-11}$, Fig. 4a), as was the mean degree (ICC = 0.92, $P = 2.11 \times 10^{-7}$, Fig. 4b) and the BC (ICC = 0.98, $P = 4.97 \times 10^{-9}$, Fig. 4f). The mean path length (ICC = 0.77, $P = 2.47 \times 10^{-4}$, Fig. 4c), mean clustering coefficient (ICC = 0.59, $P = 8.33 \times 10^{-3}$, Fig. 4d), and the small world property (ICC = 0.60, $P = 0.007$, Fig. 4e) were also reproducible, supporting the robustness of the method for the number of nodes, the mean degree, and the BC and demonstrating moderate reliability for the mean path length, mean clustering coefficient, and the small world property. The reproducibility of the degree, average minimum path length, and the betweenness coefficient might reflect their relationship with the number of nodes.

Discussion

We have presented a new method to statistically describe gray matter from individual T_1-weighted MRI scans. The method was used to construct networks for individual cortices, where the nodes represented small 3D areas that were connected by computing intracortical similarities in gray matter morphology. With the use of simple statistics from graph theory, we found that all networks had the small world property because they had a higher clustering coefficient than random networks and a similar minimum path length. All individual networks also showed intersubject variability that was most evident in the spatial distributions of the degree values. The values of the clustering and small world coefficients were similar to other morphological networks measured at a comparable sparsity level (He, Chen, et al. 2007, 2008; Bassett et al. 2008; Sanabria-Diaz et al. 2010; Yao et al. 2010). All network property values were highly similar to 2 resting-state functional MRI networks of comparable size and sparsity (van den Heuvel et al. 2008; Fornito et al. 2010). However, in comparison to the other functional (Eguíluz et al. 2005; Zhang et al. 2009, 2010; Hayasaka and Laurienti 2010) and white matter MRI studies (Hagmann et al. 2007; Zalesky et al. 2010), all the property values (apart from the clustering coefficient) were lower in the present networks. Finally, the graph theoretic properties were reproducible, supporting the robustness of the method.

Spatial Distribution of Hubs

The spatial distribution of the hubs (nodes with a high degree) in our networks showed a striking similarity with the spatial distribution of hubs based on correlations in cortical thickness (Lerch et al. 2006). It is important to note that in our study, the spatial distribution of degree values was measured for each individual separately, while the cortical thickness study computed correlations between anatomical areas using observations from different people. Possibly, the similarity of gray matter morphology within an individual brain could contribute to cortical thickness correlations found in the group data.

In the present study, the hubs were mostly located along the cortical midline. This spatial distribution has a remarkable

Table 2

Hub regions based on degree and BC and comparison with previous studies

Area	Av. % hubs	Av. BC ×10⁻⁴	Av. deg ×10⁻³	Other studies
CINGr	11.98	1.99	2.76	b2, c2
SFGr	11.76	1.8	2.75	a1, b1, b2, c1,c2, c3
SFGl	11.23	1.77	2.74	a1, b1, b2, c3
MFGl	10.41	2.19	2.74	a1, a2, b2
MFGr	9.89	1.84	2.73	a1, a2, b1, b2, c2
stTGl	9.18	2.05	2.74	a1, b2
CINGl	8.49	1.96	2.73	a2, c2
MidFGr	8.1	2.14	2.74	a1, a2, c2, c3
stTGr	7.7	1.93	2.74	a1, c1,b3
MidFGl	7.28	1.74	2.75	a1, a2, b2, c2, c3
IFGl	7.06	1.55	2.73	a1, a2, c1, c2, c3
IFGr	6.96	1.59	2.74	a1, c2, c3
MTGl	6.84	1.9	2.72	a1, a2, b2, c3
MTGr	6.5	1.94	2.75	a1, a2, b2, c1, c2, c3
PRcGl	4.78	1.48	2.74	a1, b2, c1, c2, c3
PRcGr	4.16	1.51	2.75	a1, b2, c1, c2, c3
INSl	4.06	1.75	2.73	b1
POcGl	3.9	2.42	2.73	a1, b2, c3
PCUr	3.81	1.52	2.75	a1, a2, b1, b2
PCUl	3.77	1.59	2.74	a1, a2, b1, b2

Note: Av. denotes average, BC, the betweenness centrality, and deg., the degree. We compared our results with a1 Functional study: Achard et al. (2006), a2 Functional study: Buckner et al. (2009), b1 DTI study: Gong et al. (2009), b2 DTI study: Iturria-Medina et al. (2008), c1 Morphological study: Chen et al. (2008), c2 Morphological study: Bassett et al. (2008), and c3 Morphological study: He, Chen, et al. (2007).
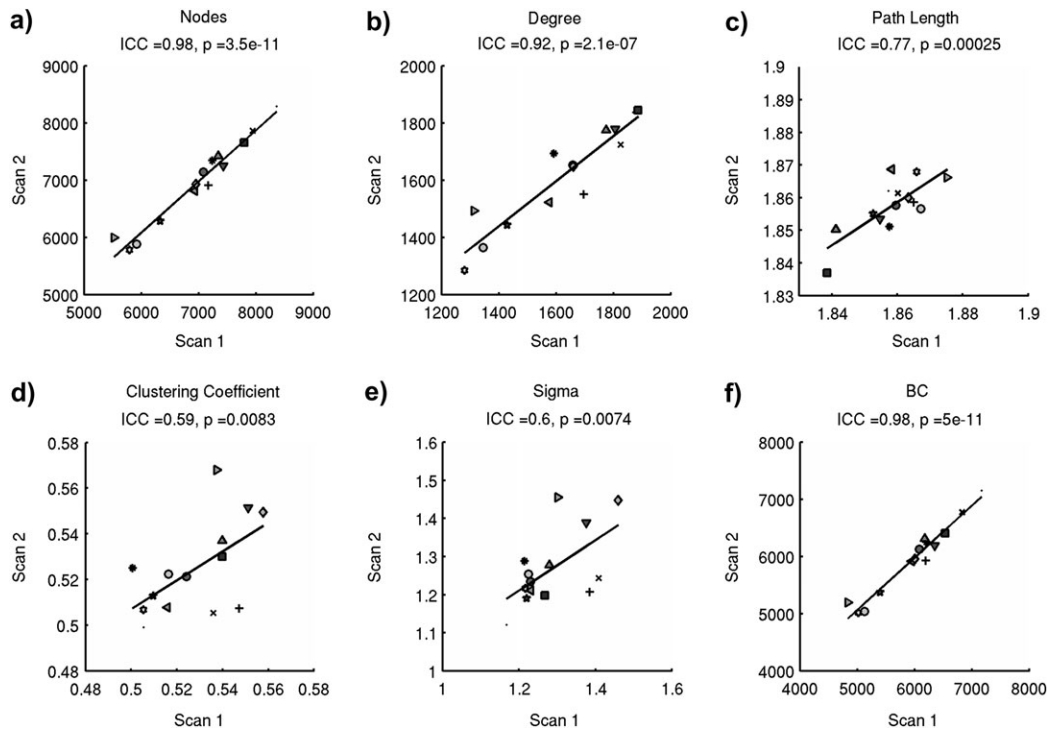
Figure 4. Reproducibility plotted for 2 scans of each subject, represented by a unique symbol and gray shade combination for all the measures: (a) the number of nodes, (b) the mean degree, (c) mean path length, (d) mean clustering coefficient, (e) the small world property (sigma), and (f) the BC. The value of the ICC is indicated above each plot, with its corresponding P value. All the measures were reproducible for a $P < 0.05$, indicating that the method is robust.

overlap with the default mode network of brain function (Raichle et al. 2001) that includes dorsal medial frontal regions (BAs 8, 9, 10, and 32), superior and middle frontal gyri (BAs 8, 9, and 10), the medial posterior cingulate (BAs 30 and 31), the precuneus (BA 7), the paracentral lobule (BA 5), inferior parietal regions (BAs 40, 39, and 7), the angular gyri (BAs 19 and 39), and inferior frontal areas (BAs 10 and 47). These regions have shown decreased activation during attention related tasks but show tonic activation during rest. Recently, robust structural connections between some of these regions were found in combined functional and DTI studies, further supporting the idea that functional connectivity might reflect structural connectivity (Skudlarski et al. 2008; Greicius et al. 2009; also see Honey et al. 2009). Our networks showed similar properties to 2 resting-state functional MRI network studies of comparable size and sparsity (van den Heuvel et al. 2008; Fornito et al. 2010), also suggesting an overlap between the organization of intracortical similarities and functional correlations in the brain. It would be interesting to investigate how similarities in gray matter morphology might be related to functional coactivation within individuals.

Intracortical Similarities

We can only speculate about the mechanisms that underlie morphological similarities in the cortex and their relationship to connectivity. One possible explanation comes from the axon tension theory proposed by van Essen (1997). He posited that axons between connected cortical areas cause a mechanical force, resulting in a tension that pulls connected areas together, whereas areas that are not connected simply drift apart. Several predictions resulting from the axon tension hypothesis have been demonstrated in monkey and human brains. Hilgetag and

Barbas (2005, 2006) showed with a series of tracer studies in monkey brains that axonal tension shifts cortical layers resulting in either thinner (heavily pulled on) or thicker cortex, as predicted by van Essen (1997). In the human brain using structural MRI, Im et al. (2006) found that cortical thickness and folding area could account for 50% of the variance in fractal dimension (i.e., an indication of repetition of structure at different spatial scales) of the cerebral cortex. They suggested that a high fractal dimension, combined with a thinner and more convoluted cortex, is in keeping with the axon tension theory. Finally, Casanova et al. (2009) reported that in comparison to controls, people with autism had a reduced gyral window, which is measured by the depth of gyral white matter and gives an indication of the space available for connections to and from the cortex. This measure was correlated with abnormalities in microcolumnar arrangement of neurons.

The above research indicates that connectivity of the brain can have an effect on its morphology. Even if intracortical similarities in gray matter morphology do not have a clear direct relationship with anatomical connectivity, it does provide a concise description of the structure of individual cortices.

Methodological Issues and Future Research

The nodes of the networks had a fixed resolution that was based on the lowest possible scale that can measure both folding and thickness (Kiselev et al. 2003), combined with a voxel size that is generally used in functional MRI studies. In future research, we want to find out how different spatial resolutions will influence the results.

Another limitation is the rigid extraction of the cubes that might not optimally correspond to the convolutions of the brain. Further studies will aim at addressing this issue.

The number of nodes and the average degree influence the network property values, as shown here and in recent studies (He, Chen, et al. 2007; Bassett et al. 2008, 2010; He et al. 2008; Fornito et al. 2010; van Wijk et al. 2010; Zalesky et al. 2010). As a consequence, the fact that the number of nodes was highly stable over time might have caused the stability of the degree, average minimum path length, and the betweenness coefficient. In general, such intricate relationships greatly complicate the comparison of networks, when everything but the network property of interest should be held constant. However, this is not always possible. With our approach, the number of nodes could not be kept constant because the subjects were analyzed in native space to keep their individual variability intact. But even when warping individual brains to a standard space where the same number of nodes are defined for all individual subjects, some nodes might not be present in their native space (or might consist of a slightly different combination of gyri and/or sulci; e.g., Paus et al. (1996) showed in a sample of 247 subjects that a small percentage of them did not have a paracingulate sulcus in either the left (8%) or the right (15%) hemisphere). In addition to the number of nodes, the number of edges in a network could be kept constant. However, such a procedure will introduce spurious connections because edges might not exist in some individuals. We tried to avoid different rates of spurious connections between individuals, by ensuring that all individual networks had the same 5% chance of spurious connections. A disadvantage of this approach is that it can result in different spatial degree distributions for all individuals. How to compare such different networks raises important methodological issues that deserve more attention (Sporns et al. 2005; Rubinov and Sporns 2010; van Wijk et al. 2010) but lie outside the scope of the present study. The present method contributes to solving these issues, by offering an approach that can be applied to different modalities to extract networks in a similar manner per individual or group.

Addition of noise to the data was limited by keeping the MRI scans in their native space, but voxels might still have been assigned to the incorrect tissue class during segmentation (e.g., due to partial volume effects). However, as the method mostly concerns the spatial relationship between voxels within small cortical areas, these errors should not have a prominent effect on the results. Addition of noise to the data was further limited by using only angles that did not require interpolation to correct for rotation when computing the correlation coefficient. A simulation study (with the use of a simplified model to represent structural MRI, see Supplementary Figure 1) estimated that approximately 1% of the similarities could have been missed using just these angles.

The spatial distribution of the degree and BC hubs showed a strong positive relationship with the size of an anatomical region. This relationship might explain why those regions have been indicated as hubs in other studies as well. This illustrates how a priori anatomical templates can influence results and that it is important to develop alternative anatomical parcellation schemes that lead to similarly sized anatomical regions (e.g., see Hagman et al. 2007; Meunier et al. 2009; Zalesky et al. 2010). Our method does not require a priori parcellation schemes, and therefore, the results can be easily projected on any other alternative.

Because the scans can be processed in their native space, the method would be particularly suited to study connectivity patterns in subtle neuropsychiatric disorders that do not show gross disruptions in brain structure. In this case, small changes or cortical abnormalities could be filtered out during warping procedures. Most importantly, now the morphology of gray matter can be described for each individual separately, while groups could be compared by averaging the descriptive statistics without the need to warp individual brains to a standard space or to use a prior model to define anatomical areas.

The subjects were scanned twice within a 6-month period, and the results indicated that network property values were stable over that period. We have interpreted this result as an indication of the robustness of the method since it was assumed that the structure of subjects' brains would be stable over such a period. However, some studies have shown that gray matter volume can change over time as a result of training or experience (Andrews et al. 1997; Draganski et al. 2004; Mechelli et al. 2004; Hyde et al. 2009; but also see Thomas et al. 2009). Even though the present study did not include any learning or training tasks, we cannot exclude that such effects might have influenced the results. It would be interesting to investigate whether the proposed method could find such subtle differences with a controlled experiment.

Our method shows some resemblance to methods that compute the fractal dimension (see e.g., Chuang et al. 1991; Bullmore et al. 1994; Free et al. 1996; Kiselev et al. 2003; Im et al. 2006; Jiang et al. 2008). Those methods result in one value per individual, the fractal dimension, which indicates whether structures are repeated at different spatial scales. By assessing intracortical similarities within a spatial scale, we have shown that it is possible to represent the morphology of the cortex as a network. An important next step would be to investigate how intracortical similarities contribute to the fractal dimension by using different spatial resolutions for the cubes.

To conclude, it would be interesting to study how changes in functional connectivity and in the morphology of the brain interact. Dysfunctional connectivity between brain regions seems to be at the core of many mental diseases, such as schizophrenia (e.g., Friston and Frith 1995; Friston 1998; Stephan et al. 2009) and autism (e.g., Belmonte et al. 2004). Although studies have established that both functional and structural MRI seem to be different in disease than in health, the interaction of structural and functional changes is not well understood. Our method could contribute to further understanding of such interactions by combining individual anatomical networks with individual functional imaging data.

Supplementary Material

Supplementary material can be found at: http://www.cercor.oxfordjournals.org/

References

Achard S, Salvador R, Whitcher B, Suckling J, Bullmore E. 2006. A resilient, low-frequency, small-world human brain functional network with highly connected association cortical hubs. J Neurosci. 26:63-72.

Albert R, Barabási AL. 2002. Statistical mechanics of complex networks. Rev Mod Phys. 74:47-97.

Andrews T, Halpern S, Purves D. 1997. Correlated size variations in human visual cortex, lateral geniculate nucleus, and optic tract. J Neurosci. 17:2859-2868.

Barbas H. 1986. Pattern in the laminar origin of corticocortical connections. J Comp Neurol. 252:415-422.

Barbas H, Rempel-Clower N. 1997. Cortical structure predicts the pattern of corticocortical connections. Cereb Cortex. 7:635-646.

Barrat A, Barthélemy M, Pastor-Satorras R, Vespignani A. 2004. The architecture of complex weighted networks. Proc Natl Acad Sci U S A. 101:3747-3752.

Bassett DS, Brown JA, Deshpande V, Carlson JM, Grafton ST. 2010. Conserved and variable architecture of human white matter connectivity. Neuroimage. 54:1262-1279.

Bassett D, Bullmore E. 2006. Small-world brain networks. Neuroscientist. 12:512-523.

Bassett D, Bullmore E, Verchinski B, Mattay V, Weinberger D, Meyer-Lindenberg A. 2008. Hierarchical organization of human cortical networks in health and schizophrenia. J Neurosci. 28:9239-9248.

Belmonte M, Allen G, Beckel-Mitchener A, Boulanger L, Carper R, Webb S. 2004. Autism and abnormal development of brain connectivity. J Neurosci. 24:9228-9231.

Benjamini Y, Hochberg Y. 1995. Controlling the false discovery rate: a practical and powerful approach to multiple testing. J R Stat Soc Series B Stat Methodol. 57:289-300.

Benjamini Y, Yekutieli D. 2001. The control of the false discovery rate in multiple testing under dependency. Ann Stat. 29:1165-1188.

Bernhardt B, Rozen D, Worsley K, Evans AC, Bernasconi N, Bernasconi A. 2009. Thalamo-cortical network pathology in idiopathic generalized epilepsy: insights from MRI-based morphometric correlation analysis. Neuroimage. 46:373-381.

Borgefors G, Nyström I, di Baja G. 1997. Connected components in 3D neighbourhoods. In: Frydrych M, Parkkinen J, Visa A, editors. Proceedings of 10th Scandinavian Conference on Image Analysis (SCIA '97). Lappeenranta (Finland): Pattern Recognition Society of Finland. p 567-572.

Buckner RL, Sepulcre J, Talukdar T, Krienen FM, Liu H, Hedden T, Andrews-Hanna JR, Sperling RA, Johnson KA. 2009. Cortical hubs revealed by intrinsic functional connectivity: mapping, assessment of stability, and relation to Alzheimer's disease. J Neurosci. 29:1860-1873.

Bullmore E, Brammer M, Harvey I, Persaud R, Murray R, Ron M. 1994. Fractal analysis of the boundary between white matter and cerebral cortex in magnetic resonance images: a controlled study of schizophrenic and manic-depressive patients. Psychol Med. 24:771-781.

Bullmore E, Sporns O. 2009. Complex brain networks: graph theoretical analysis of structural and functional systems. Nat Rev Neurosci. 10:186-198.

Casanova MF, El-Baz A, Mott M, Mannheim G, Hassan H, Fahmi R, Giedd J, Rumsey JM, Switala AE, Farag A. 2009. Reduced gyral window and corpus callosum size in autism: possible macroscopic correlates of a minicolumnopathy. J Autism Dev Disord. 39: 751-764.

Chen ZJ, He Y, Rosa-Neto P, Germann J, Evans AC. 2008. Revealing modular architecture of human brain structural networks by using cortical thickness from MRI. Cereb Cortex. 18:2374-2381.

Chuang KS, Valentino DJ, Huang HK. 1991. Measurement of fractal dimension using 3D technique. Proc SPIE Image Process. 1445: 341-347.

Colibazzi T, Zhu H, Bansal R, Schultz RT, Wang Z, Peterson BS. 2008. Latent volumetric structure of the human brain: exploratory factor analysis and structural equation modeling of gray matter volumes in healthy children and adults. Hum Brain Mapp. 29:1302-1312.

Dijkstra EW. 1959. A note on two problems in connexion with graphs. Num Mat. 1:269-271.

Dombrowski S, Hilgetag C, Barbas H. 2001. Quantitative architecture distinguishes prefrontal cortical systems in the rhesus monkey. Cereb Cortex. 11:975-988.

Draganski B, Gaser C, Busch V, Schuierer G, Bogdahn U, May A. 2004. Neuroplasticity: changes in grey matter induced by training. Nature. 427:311-312.

Eguíluz VM, Chialvo DR, Cecchi GA, Baliki M, Apkarian AV. 2005. Scale-free brain functional networks. Phys Rev Lett. 94:018102.

Fornito A, Zalesky A, Bullmore ET. 2010. Network scaling effects in graph analytic studies of human resting-state FMRI data. Front Syst Neurosci. 4:22.

Fransson P, Åden U, Blennow M, Lagercrantz H. 2011. The functional architecture of the infant brain as revealed by resting-state fMRI. Cereb Cortex. 21:145-154.

Free SL, Sisodiya SM, Cook MJ, Fish DR, Shorvon SD. 1996. Three-dimensional fractal analysis of the white matter surface from magnetic resonance images of the human brain. Cereb Cortex. 6:830-836.

Freeman LC. 1977. A set of measures of centrality based on betweenness. Sociometry. 40:35-41.

Friston KJ. 1998. The disconnection hypothesis. Schizophr Res. 30: 115-125.

Friston KJ, Frith CD. 1995. Schizophrenia: a disconnection syndrome? Clin Neurosci. 3:89-97.

Gong G, He Y, Concha L, Lebel C, Gross DW, Evans AC, Beaulieu C. 2009. Mapping anatomical connectivity patterns of human cerebral cortex using in vivo diffusion tensor imaging tractography. Cereb Cortex. 19:524-536.

Gountouna VE, Job DE, McIntosh AM, Moorhead TWJ, Lymer GKL, Whalley HC, Hall J, Waiter GD, Brennan D, McGonigle DJ, et al. 2010. Functional Magnetic Resonance Imaging (fMRI) reproducibility and variance components across visits and scanning sites with a finger tapping task. Neuroimage. 49:552-560.

Greicius MD, Supekar K, Menon V, Dougherty RF. 2009. Resting-state functional connectivity reflects structural connectivity in the default mode network. Cereb Cortex. 19:72-78.

Hagmann P, Kurant M, Gigandet X, Thiran P, van Wedeen J, Meuli R, Thiran JP. 2007. Mapping human whole-brain structural networks with diffusion MRI. PLoS One. 2:e597.

Hayasaka S, Laurienti PJ. 2010. Comparison of characteristics between region- and voxel-based network analyses in resting-state fMRI data. Neuroimage. 50:499-508.

He Y, Chen Z, Evans A. 2008. Structural insights into aberrant topological patterns of large-scale cortical networks in Alzheimer's disease. J Neurosci. 28:4756-4766.

He Y, Chen ZJ, Evans AC. 2007. Small-world anatomical networks in the human brain revealed by cortical thickness from MRI. Cereb Cortex. 17:2407-2419.

He Y, Wang L, Zang Y, Tian L, Zhang X, Li K, Jiang T. 2007. Regional coherence changes in the early stages of Alzheimer's disease: a combined structural and resting-state functional MRI study. Neuroimage. 35:488-500.

Hilgetag CC, Barbas H. 2005. Developmental mechanics of the primate cerebral cortex. Anat Embryol (Berl). 210:411-417.

Hilgetag CC, Barbas H. 2006. Role of mechanical factors in the morphology of the primate cerebral cortex. PLoS Comput Biol. 2:146-159.

Honey CJ, Sporns O, Cammoun L, Gigandet X, Thiran JP, Meuli R, Hagmann P. 2009. Predicting human resting-state functional connectivity from structural connectivity. Proc Natl Acad Sci U S A. 106: 2035-2040.

Humphries MD, Gurney K, Prescott TJ. 2006. The brainstem reticular formation is a small-world, not scale-free, network. Proc R Soc B Biol Sci. 273:503-511.

Hyde KL, Lerch J, Norton A, Forgeard M, Winner E, Evans AC, Schlaug G. 2009. Musical training shapes structural brain development. J Neurosci. 29:3019-3025.

Im K, Lee JM, Yoon U, Shin YW, Hong SB, Kim IY, Kwon JS, Kim SI. 2006. Fractal dimension in human cortical surface: multiple regression analysis with cortical thickness, sulcal depth, and folding area. Hum Brain Mapp. 27:994-1003.

Iturria-Medina Y, Sotero RC, Canales-Rodriguez EJ, Aleman-Gomez Y, Melie-Garcia L. 2008. Studying the human brain anatomical network via diffusion-weighted MRI and Graph Theory. Neuroimage. 40:1064–1076.

Jiang J, Zhu W, Shi F, Zhang Y, Lin L, Jiang T. 2008. A robust and accurate algorithm for estimating the complexity of the cortical surface. J Neurosci Methods. 172:122-130.

Kennedy D, Lange N, Makris N, Bates J. 1998. Gyri of the human neocortex: an MRI-based analysis of volume and variance. Cereb Cortex. 8:372-384.

Kiselev V, Hahn K, Auer D. 2003. Is the brain cortex a fractal? Neuroimage. 20:1765-1774.

Lerch J, Worsley K, Shaw W, Greenstein D, Lenroot R, Gledd J, Evans A. 2006. Mapping anatomical correlations across cerebral cortex (MACACC) using cortical thickness from MRI. Neuroimage. 31:993-1003.

Lewis JP. 1995. Fast normalized cross-correlation. Proc Vision Interface. Available from: http://citeseerx.ist.psu.edu/viewdoc/download?doi=10.1.1.21.6062&rep=rep1&type=pdf. Last accessed: Aug 8th 2011.

Liu Y, Liang M, Zhou Y, Hao Y, Song M, Yu C, Liu H, Liu Z, Jiang T. 2008. Disrupted small-world networks in schizophrenia. Brain. 131:945-961.

Luce RD, Perry AD. 1949. A method of matrix analysis of group structures. Psychometrika. 14:95-116.

Maslov S, Sneppen K. 2002. Specificity and stability in topology of protein networks. Science. 296:910-913.

McAlonan GM, Cheung V, Cheung C, Suckling J, Lam GY, Tai KS, Yip L, Murphy DGM, Chua SE. 2005. Mapping the brain in autism. A voxel-based MRI study of volumetric differences and intercorrelations in autism. Brain. 128:268-276.

McGraw KO, Wong SP. 1996. Forming inferences about some intraclass correlation coefficients. Psychol Methods. 1:30-46.

Mechelli A, Crinion J, Noppeney U, O'Doherty J, Ashburner J, Frackowiak R, Price C. 2004. Structural plasticity in the bilingual brain: proficiency in a second language and age at acquisition affect grey-matter density. Nature. 431:757.

Mechelli A, Friston K, Frackowiak R, Price C. 2005. Structural covariance in the human cortex. J Neurosci. 25:8303-8310.

Meunier D, Lambiotte R, Fornito A, Ersche KD, Bullmore ET. 2009. Hierarchical modularity in human brain functional networks. Front Neuroinform. 3:37.

Milgram S. 1967. The small-world problem. Psychol Today. 1:61-67.

Mitelman SA, Shihabuddin L, Brickman AM, Buchsbaum MS. 2005. Cortical intercorrelations of temporal area volumes in schizophrenia. Schizophr Res. 76:207-229.

Modinos G, Vercammen A, Mechelli A, Knegtering H, Mcguire PK, Aleman A. 2009. Structural covariance in the hallucinating brain: a voxel-based morphometry study. J Psychiatry Neurosci. 34:465-469.

Moorhead T, Gountouna V, Job D, McIntosh AM, Romaniuk L, Lymer GKS, Whalley HC, Waiter GD, Brennan D, Ahearn TS, et al. 2009. Prospective multi-centre voxel based morphometry study employing scanner specific segmentations: procedure development using CaliBrain structural MRI data. BMC Med Imaging. 9:8-19.

Newman MEJ. 2003. The structure and function of complex networks. SIAM Rev. 45:167-256.

Nikou C, Heitz F, Armspach J. 1999. Robust voxel similarity metrics for the registration of dissimilar single and multimodal images. Pattern Recognit. 32:1351-1368.

Noble WS. 2009. How does multiple testing correction work? Nat Biotechnol. 27:1135-1137.

Ourselin S, Roche A, Prima S, Ayache N. 2000. Block matching: a general framework to improve robustness of rigid registration of medical images. In: DiGioia AM, Delp S, editors. Third international conference on medical robotics, imaging and computer assisted surgery (MICCAI 2000). Pittsburgh (PA): Springer. p. 557-566.

Paus T, Tomaiulo F, Otaky N, MacDonald D, Petrides M, Atlas J, Morris R, Evans AC. 1996. Human cingulate and paracingulate sulci: pattern, variability, asymmetry and probabilistic map. Cereb Cortex. 6:207-214.

Penney GP, Griffin LD, King AP, Hawkes DJ. A novel framework for multi-modal intensity-based similarity measures based on internal similarity. In: Reinhardt JM, Pluim JPW, editors. SPIE Medical Imaging 2008: Image Processing. San Diego (CA): SPIE. Abstract number: 69140X.

Pezawas L, Verchinski B, Mattay V, Callicott J, Kolachana B, Straub R, Egan M, Meyer-Lindenberg A, Weinberger D. 2004. The brain-derived neurotrophic factor val66met polymorphism and variation in human cortical morphology. J Neurosci. 24:10099-10102.

Raichle M, MacLeod A, Snyder A, Powers W, Gusnard D, Shulman G. 2001. A default mode of brain function. Proc Natl Acad Sci U S A. 98:676-682.

Rubinov M, Sporns O. 2010. Complex measures of brain connectivity: uses and interpretations. Neuroimage. 52:1059-1069.

Sanabria-Diaz G, Melie-García L, Iturria-Medina Y, Alemán-Gómez Y, Hernández-González G, Valdés-Urrutia L, Galán L, Valdés-Sosa P. 2010. Surface area and cortical thickness descriptors reveal different attributes of the structural human brain networks. Neuroimage. 50:1497-1510.

Skudlarski P, Jagannathan K, Calhoun VD, Hampson M, Skudlarska BA, Pearlson G. 2008. Measuring brain connectivity: diffusion tensor imaging validates resting state temporal correlations. Neuroimage. 43:554-561.

Sporns O, Chialvo DR, Kaiser M, Hilgetag CC. 2004. Organization, development and function of complex brain networks. Trends Cogn Sci. 8:418-425.

Sporns O, Tononi G, Kötter R. 2005. The human connectome: a structural description of the human brain. PLoS Comput Biol. 1:0245-0251.

Sporns O, Zwi JD. 2004. The small world of the cerebral cortex. Neuroinformatics. 2:145-162.

Stephan K, Friston K, Frith C. 2009. Dysconnection in schizophrenia: from abnormal synaptic plasticity to failures of self-monitoring. Schizophr Bull. 35:509-527.

Telesford QK, Morgan AR, Hayasaka S, Simpson SL, Barrett W, Kraft RA, Mozolic JL, Laurienti PJ. 2010. Reproducibility of graph metrics in fMRI networks. Front Neuroinform. 4:117.

Thomas AG, Marrett S, Saad ZS, Ruff DA, Martin A, Bandettini PA. 2009. Functional but not structural changes associated with learning: an exploration of longitudinal voxel-based morphometry (VBM). Neuroimage. 48:117-125.

Thompson PM, Lee AD, Dutton RA, Geaga JA, Hayashi KM, Eckert MA, Bellugi U, Galaburda AM, Korenberg JR, Mills DL, et al. 2005. Abnormal cortical complexity and thickness profiles mapped in Williams syndrome. J Neurosci. 25:4146-4158.

Tzourio-Mazoyer N, Landeau B, Papathanassiou D, Crivello F, Etard O, Delcroix N, Mazoyer B, Joliot M. 2002. Automated anatomical labeling of activations in SPM using a macroscopic anatomical parcellation of the MNI MRI single-subject brain. Neuroimage. 15:273-289.

van Court T, Gu Y, Herbordt MC. 2005. Three-dimensional template correlation: object recognition in 3D voxel data. In: di Gesù V, Tegolo D, editors. Proc 7th Intern Workshop on Computer Architecture for Machine Perception. CAMP '05. Washington (DC): IEEE Computer Society. p. 153-158.

van den Heuvel MP, Stam CJ, Boersma M, Hulshoff Pol HE. 2008. Small-world and scale-free organization of voxel-based resting-state functional connectivity in the human brain. Neuroimage. 43:528-539.

van den Heuvel MP, Stam CJ, Kahn RS, Huslhoff Pol HE. 2009. Efficiency of functional brain networks and intellectual performance. J Neurosci. 29:7619-7624.

van Essen D. 1997. A tension-based theory of morphogenesis and compact wiring in the central nervous system. Nature. 385:313-318.

van Wijk BCM, Stam CJ, Daffertshofer A. 2010. Comparing brain networks of different size and connectivity density using graph theory. PLoS One. 5:e13701.

Watts D, Strogatz S. 1998. Collective dynamics of "small-world" networks. Nature. 393:440-442.

Weese J, Rösch P, Netsch T, Blaffert T, Quist M. 1999. Gray-value based registration of CT and MR images by maximization of local correlation. In: Taylor CJ, Colchester ACF, editors. Medical image computing and computer-assisted intervention—MICCAI'99. Cambridge (UK): Springer. p. 656–663.

Wright I, Sharma T, Ellison Z, Mcguire P, Friston K, Brammer M, Murray R, Bullmore E. 1999. Supra-regional brain systems and the neuropathology of schizophrenia. Cereb Cortex. 9:366–378.

Yao Z, Zhang Y, Lin L, Zhou Y, Xu C, Jiang T. The Alzheimer's Disease Neuroimaging initiative 2010. Abnormal cortical networks in mild cognitive impairment and Alzheimer's disease. PLoS Comput Biol. 6:e1001006.

Yuan K, Qin W, Liu J, Guo Q, Dong M, Sun J, Zhang Y, Liu P, Wang W, Wang Y, et al. 2010. Altered small-world brain functional networks and duration of heroin use in male abstinent heroin-dependent individuals. Neurosci Lett. 477:37–42.

Zalesky A, Fornito A, Harding IH, Cocchi L, Yücel M, Pantelis C, Bullmore ET. 2010. Whole-brain anatomical networks: does the choice of nodes matter? Neuroimage. 50:970–983.

Zhang F, Chen C, Jiang L. 2010. Brain functional networks analysis and comparison. 3rd Proc Int Conf Biomed Eng Inform. 7:1151–1155.

Zhang F, Jiang L, Chen C, Dong Q, Yan L. 2009. Brain functional networks involved in finger movement. In: Shi R, Fu W, Wang Y, Wang H, editors. 2nd Proc Int Conf Biomed Eng Inform. Tianjin (China): IEEE. p. 1–4.

Zhu W, Wen W, He Y, Xia A, Anstey KJ, Sachdev P. 2010. Changing topological patterns in normal aging using large-scale structural networks. Neurobiol Aging. Epub ahead of print.